PERGAMON

Continental Shelf Research 18 (1998) 1517–1529

CONTINENTAL SHELF RESEARCH

A preliminary study on the internal tides of the gulfs of Patras and Korinthos, Greece

P.G. Drakopoulos*, A. Lascaratos

Laboratory of Meteorology, Department of Applied Physics, University of Athens, Greece

Received 21 April 1995; received in revised form 6 Febraury 1998; accepted 21 April 1998

Abstract

The semi-diurnal baroclinic tide in the semi-closed channel which lies between the Greek Mainland and Peloponnesus has been investigated. It appears to be generated in the centre of the channel, where a bottom step topography exists. At a location 8 km away from the source, its amplitude reaches 3 m during spring tides. Modal decomposition of the baroclinic tide indicated that the first mode accounts for 80% of the energy while almost all of the energy is accounted for by the first three vertical modes. During the observational period several upwelling events occurred. These events caused baroclinic tidal energy to disappear through the weakening of the stratification within 10–20 h. The higher modes dissipated much faster than the first mode which continued to gain energy until the isopycnal tilt reached a maximum. The available set of data indicates that the baroclinic oscillations may not be an internal Kelvin-type wave.

1. Introduction

The water body which lies between the Greek mainland to the north and Peloponnesus to the south, has the appearance of an east–west oriented semi-closed channel (Fig. 1). The western portion of this channel consists of the relatively shallow Gulf of Patras with mid-channel depths around 100 m and width 20 km. The eastern portion is the much deeper Gulf of Korinthos with depths exceeding 900 m and width varying from 10 to 30 km. In between the two gulfs lies the Bay of Navpaktos and it is there where the bottom starts deepening (the region between R1 and CH in Fig. 1). The Gulf of Navpaktos is connected to the Gulf of Patras through the Strait of Rio which has

* Correspondence address: Institute of Marine Biology of Crete, P.O. Box 2214, 71003 Iraklio, Crete, Greece.

0278–4343/98/$ – See front matter
PII: S0278–4343(98)00052–1

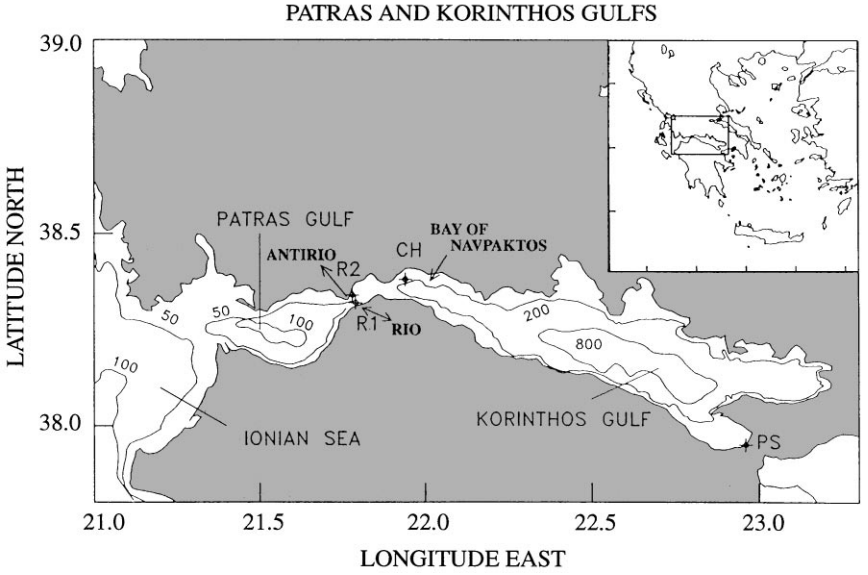

Fig. 1. General map of the area under investigation.

a width less than 3 km. Although the circulation in the channel is predominantly wind-driven, the tidal flow component is also important.

The internal (baroclinic) tides result from the interaction of the surface (barotropic) tidal wave with the bottom topography (e.g. Wunsch 1975). In the open ocean the internal tide behaves as a travelling Poincaré wave; however, when lateral bounds are present, as for example, in a channel or estuary, there is no lateral motion and the internal wave behaves as a Kelvin wave propagating away from the generation region (Forrester, 1974). At the Strait of Rio tidal velocities exceed 80 cm s^{-1} during spring tides. The presence of strong surface tides combined with the bottom step topography (100 m depth for the western sub-basin vs 900 m depth for the eastern sub-basin), create conditions that can lead to the generation of internal tides in the channel.

The present work provides, for the first time, evidence for the existence of semi-diurnal baroclinic tides near the Strait of Rio. It furthers explores the generation and propagation characteristics of the observed variability and its modification under the influence of upwelling events. Because of the short period of observations available the analysis has a rather tentative character.

2. Data

The primary source of data used in this analysis was a thermistor chain. The chain consisted of 11 thermistors spaced every 5 m, spanning the depth region from 12 to

62 m. It was deployed from 26/6/86 to 30/7/86, southeast of Navpaktos and off the still of Chiliadou at a depth of 73 m (location CH, Fig. 1). Current and temperature records from six Aanderaa current meters from two moorings R1 and R2 located 15 km west of mooring CH near the entrance of the channel, were also incorporated in this analysis (Fig. 1). Station R1 which was deployed at 66 m depth near Cape Rio, consisted of three Aanderaa current meters at depths 15, 30 and 63 m. Station R2 was deployed at 58 m depth near Cape Antirio and consisted of three current meters moored at depths 12, 25 and 55 m. Sea level data, for the same period from the permanent tidal gauge station at the port of Posidonia (PS in Fig. 1) were also used. An anemometer placed near location R1 was also monitored in order to investigate the degree of correlation between the wind forcing and upwelling. The sea level data were corrected for atmospheric pressure by using nearby pressure recorders and assuming an inverse barometer effect.

3. Methods

The barotropic and baroclinic tidal parameters (i.e. velocities, elevations and their respective phases) were deduced from current and temperature records by using standard harmonic analysis procedures (Foreman, 1977). All phase lags presented here correspond to local DST (+3 h). Most of the recorded current meter and thermistor variance was due to the semidiurnal tidal motions. Band-pass filtering of the current and temperature time series, at about 0.08 cph, revealed nonstationarity and a temporal variability not related to that of the spring-neap tidal cycle. Hence, the hourly records were segmented in 15 day intervals, (minimum interval needed for the separation of the M2 from the S2 component), having a 14 day overlapping (Drakopoulos and Marsden 1993). Using this technique it was possible to extract 18 pairs of daily tidal coefficients (u_0, g_u for the current along the major axis, and T_0, g_t for the temperature), spanning the period from 26/6/86 to 30/7/86. The corresponding degrees of freedom were 4.3.

Temperature fluctuations reflect vertical baroclinic motions. Following standard practice (Drakopoulos and Marsden, 1993) and assuming incompressibility, the vertical amplitude of the baroclinic wave can be expressed as

$$\eta \approx \frac{T_0 \cos(\omega t - g_t - \pi)}{\partial \bar{T} / \partial z} \tag{1}$$

where the overbar denotes time average. In this work the harmonic analysis residual constant term was used. This term represents a 15 day average which is identical to the window used to obtain T_0. This way spurious spikes that could be introduced by the division process were avoided. An additional requirement for the validity of Eq. (1) is that no horizontal gradient of the temperature exists. The horizontal gradient may become significant during upwelling events. During Julian days 196 and 197 (15 and 16 July 1986) there was no upwelling present, and the water body appeared to be well stratified (see Fig. 2c and d). Therefore, the values of the vertical amplitude for these days were used in the evaluation of Eq. (1).

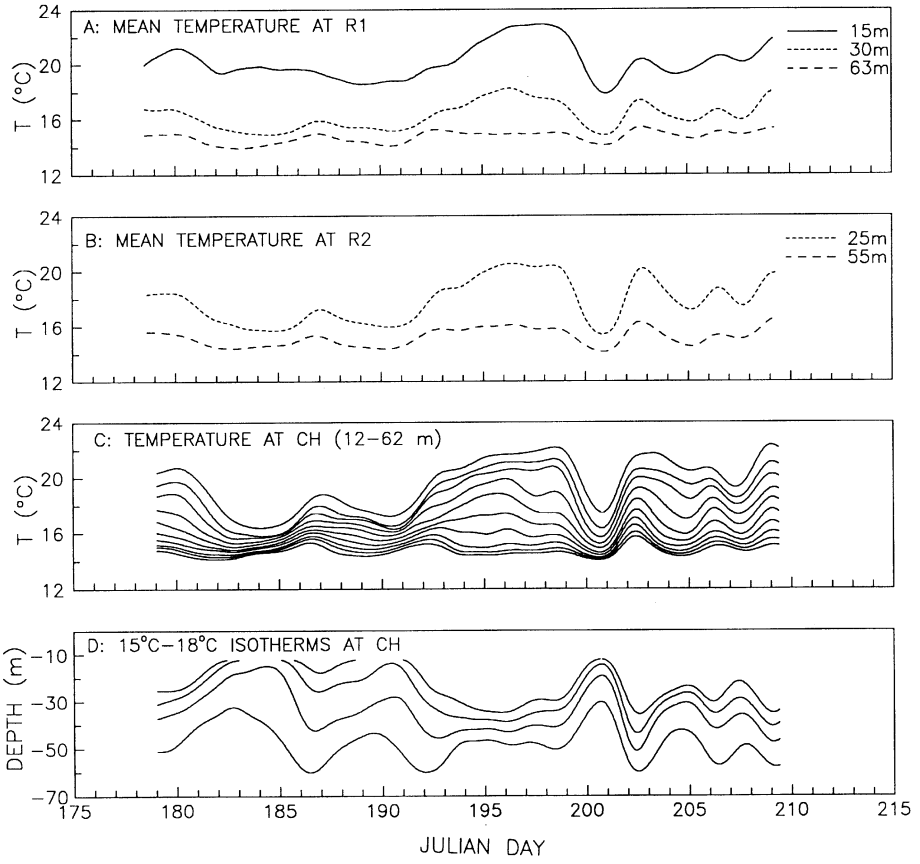

Fig. 2. Low-pass temperature fluctuations during the period of present analysis (a) at mooring R1, (b) at mooring R2, (c) at mooring CH and (d) depth of the 15, 16, 17, 18°C isotherms at the same location.

To separate barotropic and baroclinic components in the current data two techniques were used. In the first approach, a vector average of the tidal coefficients at different depths is taken. This process tends to cancel out the baroclinic contributions which are expected to have a sinusoidal vertical profile. An additional step includes temporal averaging of the coefficients, anticipating that the baroclinic contributions will be lessened further due to their randomness.

Modal decomposition was the second technique used. The vertical eigenfunctions of the Sturm-Liouville equation were fitted to the harmonic tidal analysis coefficients by means of least-squares methods. Therefore, a mooring consisting of m current meters yields the parameters for the barotropic and up to m^{-1} baroclinic components. In this work the eigenfunction problem was solved numerically by supplying as input the depth at a particular current meter location and the vertical profile of the buoyancy frequency. As three temperature readings were available only for each

current meter mooring, data from the thermistor chain (which were found to be similar) were used for the determination of N. This approach is not unreasonable as the eigenfunctions are not sensitive to the buoyancy frequency.

The modal decomposition procedure included the following steps: For a given mooring including m current meters, a system of $n(n \leqslant m)$ equations of the type:

$$\sum_i \left(\frac{\vartheta\psi_{n-1}}{\vartheta z}\right)_i u_{oi} \exp(\mathrm{i}g_{ui}) = \sum_j \left(\frac{\vartheta\psi_j}{\vartheta z}\right)_j \left(\frac{\vartheta\psi_{n-1}}{\vartheta z}\right)_j a_j \frac{\omega}{k} \exp(\mathrm{i}\theta_j) \tag{2}$$

was solved. Here $i = (1, \ldots, m)$, $j = (0, n-1)$, u_{oi} and g_{ui} represent amplitudes and phases along the major axis of the current as obtained from the daily harmonic analysis for the ith current meter. The ψ_j's are the vertical eigenfunctions while a_j and θ_j represent fitted parameters.

Similarly, the elevation parameters η_0, g_η for station CH were also obtained by solving the system:

$$\sum_i (\psi_{n-1})_i \eta_{oi} \exp(\mathrm{i}g_{ni}) = \sum_j (\psi_j)_i (\psi_{n-1})_i a_j \exp(\mathrm{i}\theta_j); \tag{3}$$

here $\psi_0 = 1 + z/H$ (the barotropic vertical dependence).

4. Results

4.1. Barotropic tides

The low-pass filtered current and wind records suggest strong wind-driven circulation near the entrance of the Gulf of Korinthos (Fig. 3). During the period of measurement most of the incoming flow enters the Gulf of Korinthos from the southern side of the strait and exits from the northern side. Wind-driven currents in the area are strong, being about $20\,\mathrm{cm\,s^{-1}}$, and some times exceeding the $40\,\mathrm{cm\,s^{-1}}$ (Fig. 3). However, even under these conditions, the Froude number for the barotropic tide is sufficiently less than unity implying that the barotropic tide should not be affected by advection.

The semidiurnal current field at moorings R1 and R2 appears to be variable due to frictional and non-linear effects in the Strait. At location R1, the amplitude for the major axis of the tidal ellipse of M2 near the surface was about $40\,\mathrm{cm\,s^{-1}}$, while at a depth of 63 m drops to below $30\,\mathrm{cm\,s^{-1}}$ due to bottom boundary layer friction. The orientation of the major axis, and thus the direction of the tidal flow, is forced to follow the isobath contours close to the bottom.

For mooring R2, the near surface tidal speed has the highest variability, while near bottom current speed remains more uniform throughout that period ($\sim 20\,\mathrm{cm\,s^{-1}}$). Similarly here, the inclination of the major axis is also forced to follow the bathymetry near bottom and is shifted northward. The amplitudes of the minor axes for all tidal current ellipses were found to be negligible. This demonstrates the absence of transverse motion, which is a characteristic property of Kelvin waves.

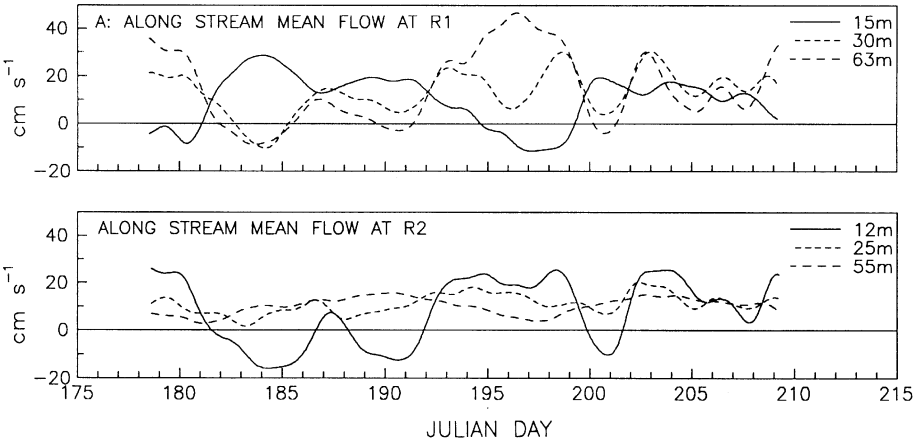

Fig. 3. Low-pass axial current components at moorings (a) R1 and (b) R2.

Table 1
Barotropic semidiurnal parameters as obtained from modal decomposition and depth averaging of tidal coefficients. Velocity amplitudes of stations R1 and R2 are expressed in cm s^{-1} and elevation for station PS is in cm. The quantity in the parenthesis represents phase lag in degrees corresponding to local time (+3)

Mooring	M_2 (modal)	M_2 (averaged)	S_2 (modal)	S_2 (averaged)
R1	40.1(73)	40.6(75)	19.2(108)	18.3(111)
R2	21.6(52)	21.0(49)	12.6(95)	12.0(92)
PS		12.0(191)		5.6(225)

The results for the barotropic field, estimated by the averaging method and the modal decomposition are presented in Table 1. Both methods agree within 4%. The ratios between S_2 and M_2 components are representative of those for the open ocean (~ 0.5). The amplitude at station R1 was found to be almost twice that at R2 (41 vs 21 cm s^{-1}). The semidiurnal barotropic elevations obtained by the harmonic analysis procedure of the tidal gauge records at PS, is also depicted in Table 1. The amplitude exceeds 17 cm during spring tides and the phase difference between current and elevation is about 100°. Spectral analysis indicated that the coherence between all barotropic modes was over 0.97 (Table 2).

4.2. Baroclinic tides

The overall behaviour of the baroclinic field appears to be intermittent (Fig. 4a). The amplitude of the first baroclinic mode of M_2 exhibits most variability. The period of measurement is too short to conclusively resolve the variability of the signal. Nevertheless, a few observations can be made. In Fig. 5a, the vertical structure of the

Table 2
Transfer functions t_{xy}, their phase lags g_{xy} and coherence squared c_{xy} between barotropic and baroclinic modes. The quantity in the parentheses is the order of the decomposed mode. The 95% significance level is 0.6

Mooring mode	t_{xy}	g_{xy}(deg)	c_{xy}
R1(0)–R2(0)	1.7	12	0.97
R1(1)–R2(1)	0.2	256	0.42
R1(1)–CH(1)	1.8	144	0.43
R2(1)–CH(1)	6.1	281	0.54
PS(0)–R1(0)	—	124	0.99
PS(0)–R2(0)	—	136	0.99
PS(0)–CH(1)	—	176	—
R1(0)–R1(1)	—	109	—
R2(0)–R2(1)	—	123	—

M_2 elevation (both experimental and fitted) is depicted for the thermistor chain station during a period of high stratification (Julian day 197). In the same figure, the elevations obtained by performing harmonic analysis directly on the isotherms are superimposed. The agreement is consistent giving validity to the gradient procedure. Using the fitted a_n and θ_n the axial velocity profile was reconstructed assuming $u_n = (\omega/k_n)\partial\eta_n/\partial z$ and is presented in Fig. 5b. The M_2 internal tide has a maximum amplitude ($\sim$2 m) at 25 m depth, which coincides with the location of the thermocline. The associated speeds are about 4 cm s^{-1} near the surface, they reduce to about 1 cm s^{-1} at the interface level and to 2.8 cm s^{-1} near the bottom. The first three out of the ten fitted modes were enough to describe the vertical structure.

Modal decomposition at mooring R2 gave amplitudes higher than R1, an indication of an outgoing internal wave. The M_2 coherence between moorings R1 and R2 for the baroclinic modes are below significance level (Table 2). Moreover, the amplitudes at R1 and R2 were found to be 2–6 times higher than CH; the discrepancy is also reflected on the amplitudes of the transfer functions (Table 2). This disagreement cannot be resolved by the present data set. Nevertheless, it is worth noting that the presence of evanescent Poincaré waves at the Strait (Brown, 1973; Middleton 1991) or the effect of the mean shear (Thomson and Huggett, 1980) provide potential explanations. Furthermore, it should be mentioned that the because the Froude number is sufficiently high at times ($\sim$0.7) even the first and more energetic mode, can be subjected to mean flow advection.

5. Discussion

A suitable location for the generation of internal tides is the area which accomodates a discontinuity of the bottom topography (e.g. continental shelf break), and the

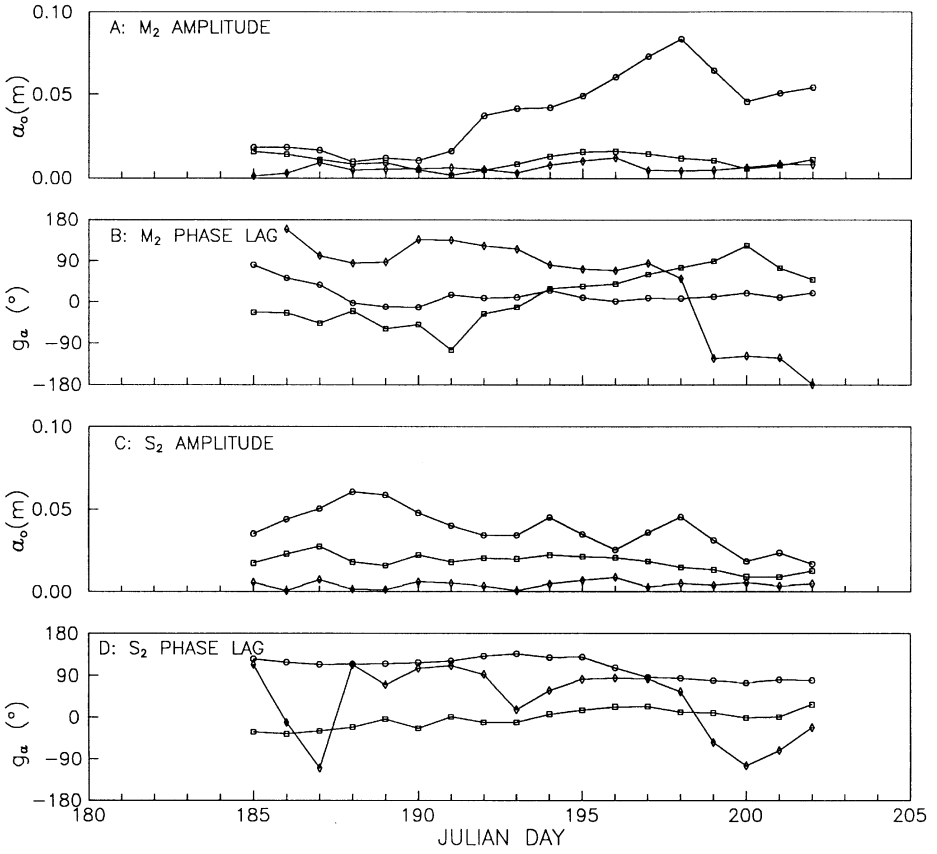

Fig. 4. Tidal coefficients for the first baroclinic modes as obtained from modal decomposition at mooring CH: (a) M_2 amplitude, (b) M_2 phase lag, (c) S_2 amplitude, and (d) S_2 phase lag. Circles represent mode 1, squares mode 2, and diamonds mode 3.

slope of characteristics $(\omega^2 - f^2)/(N^2 - \omega^2)$ matches that of the bottom (Baines, 1974). In the channel under investigation, such a place exists near the Bay of Navpaktos (location CH, Fig. 1). Directional spectrum analysis required to locate the generation region is prohibited by the limited amount of available data. However, a simple examination of the phase relationship between the barotropic mode and first baroclinic mode can provide the radius of a circle where possible generation regions lie. The horizontal wave number is related to the distance through the relationship $\Delta x = \Delta g_n / k_n$. Since the barotropic elevation mode is a standing wave, the tidal phase at station PS can safely assumed to be the same everywhere in the channel. Then, using the resulting wave numbers (time average) of the eigenvalue problem solution, the distance Δx was computed. The phase lag was obtained from the complex transfer function between station PS and the 1st mode of station CH. The phase relationship between the barotropic mode and the first baroclinic mode of moorings R1 and R2

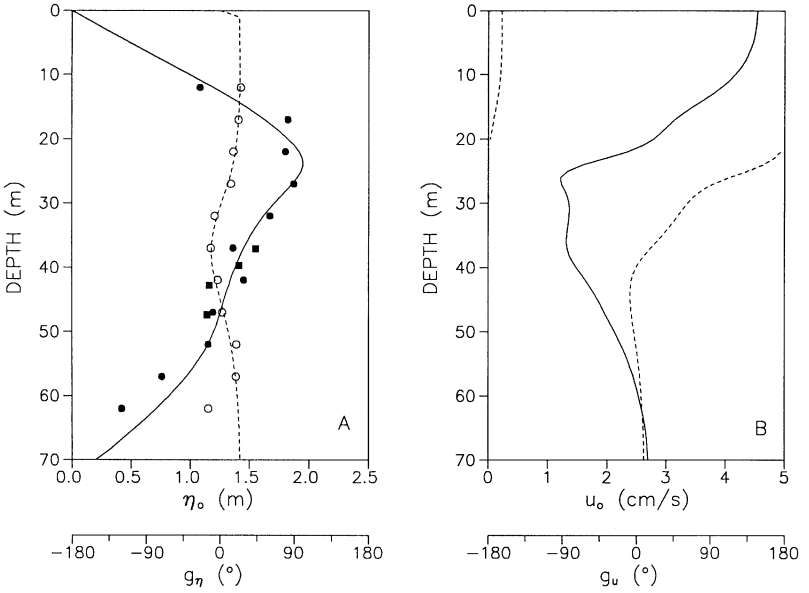

Fig. 5. Vertical structure of M_2 baroclinic tide at mooring CH: (a) elevation, (b) velocity. Solid circles are experimental values obtained from gradient procedure. Solid squares are experimental values obtained separately by harmonic analysis on the isotherms. Similarly shaped light points are their corresponding phases. Solid lines are least squares fitted amplitudes. Dashed lines are the corresponding fitted phases.

Table 3
Phase difference between first baroclinic and barotropic mode, corresponding time-averaged wave number and expected distance between generation and observation locations

Mooring	$\Delta g(^\circ)$	$k_1(\mathrm{m}^{-1})$	Δx (km)
CH	176	3.7×10^{-4}	8.3
R1	109	4.0×10^{-4}	4.8
R2	123	4.0×10^{-4}	5.4

were obtained again from the corresponding complex transfer function. The results are presented in Table 3. The above procedure gave for station CH a distance of 8.3 km which is roughly the location of the bottom break near Navpaktos. Similarly the distance corresponding to moorings R1 and R2 is 4.8 and 5.4 km, respectively, and is again located very close to the same generation area.

A rough estimate of the energetics of the tidal field during day 196, which is considered typical, gave a value for the baroclinic power of about 1.0×10^6 W, while for the barotropic component 1.5×10^8 W, two orders of magnitude higher. Therefore,

in this channel, for this period of measurements, the baroclinic field is not a major mechanism for the dissipation of the barotropic power.

The morphology of the area around the Strait of Rio enhances the conditions for the generation of upwelling. The steep mountains on both sides at the entrance of the Bay of Navpaktos funnel the frequent northwesterly to southwesterly winds in an axial direction. Thus, although the wind blowing outside the channel during the month of July was northwesterly, the anemometer in the Strait registered maximum intensity in the axial direction (WSW) which favours upwelling along the northern side of the Bay of Navpaktos and Gulf of Korinthos.

The depth of the 16°C isotherm was selected as an indicator for the baroclinic processes in location CH, since its vertical movement was registered by the thermistors throughout the period of investigation. During calm wind conditions it lies at a depth of 44 m, below the thermocline which can be found at about 25 m. Singular Spectrum Analysis(SSA) was used to break the time series into modes (Vautard et al., 1992). The SSA decomposition of the isotherm record consisted mainly of an aperiodic component incorporating the upwelling events, a semidiurnal doublet, and a near-inertial doublet. The amplitudes for the periodic processes (tides), were deduced by applying complex demodulation on the corresponding SSA components.

The peeks of the record are indications of upwelling events (Fig. 6d). Depending on the stratification, the records can be divided in three parts. From day 180 to 194, 194 to 199 and 199 to 209 (see Fig. 2d). During the first part, the stratification is weak due to persisting winds, and two upwelling events are present (peak on days 184 and 190). During the second part, the wind weakens, the semidiurnal currents are minimum (neap tides, Fig. 6f) and the water column is well stratified. Finally, during the last part three upwelling events are present (days 201, 205, 208), but the stratification remains high at least during the first episode. The first upwelling event had the longest duration with spin-up time of 7 days, and the third event the highest vertical velocity of about $0.01\,\mathrm{cm\,s^{-1}}$. During this event, and because of the wind flow direction reversal, downwelling occurred with a vertical speed of $0.02\,\mathrm{cm\,s^{-1}}$ (Fig. 6a and d).

The effect which the upwelling has on the semidiurnal baroclinic motions can be readily observed by comparing the aperiodic and the demodulated semidiurnal SSA components of the 16°C isotherm (Fig. 6d and e). Their respective variabilities are almost 180- out of phase. Maximum internal tide amplitudes occur when the isotherm lies on its equilibrium position (at 44 m depth). Both during upwelling and downwelling, the semidiurnal amplitude is attenuated or diminished (e.g. days 185 and 201). This happens although the forcing during these days is almost maximum because of the presence of spring tides (Fig. 6f). The response time of the internal tide to the stratification variability can be assessed from the time series of Fig. 6. The amplitude minima of the internal tide occur at about 10–20 h after the corresponding upwelling maxima. Even if the modulation of the internal tide was occurring at the source region, 7 km west of CH, it takes about 6 h for mode 1, which is the fastest ($u_g = 0.38\,\mathrm{m\,s^{-1}}$), to reach location CH. Therefore, the additional time lag should be due to the time needed for the semidiurnal baroclinic field to adjust to the new stratification.

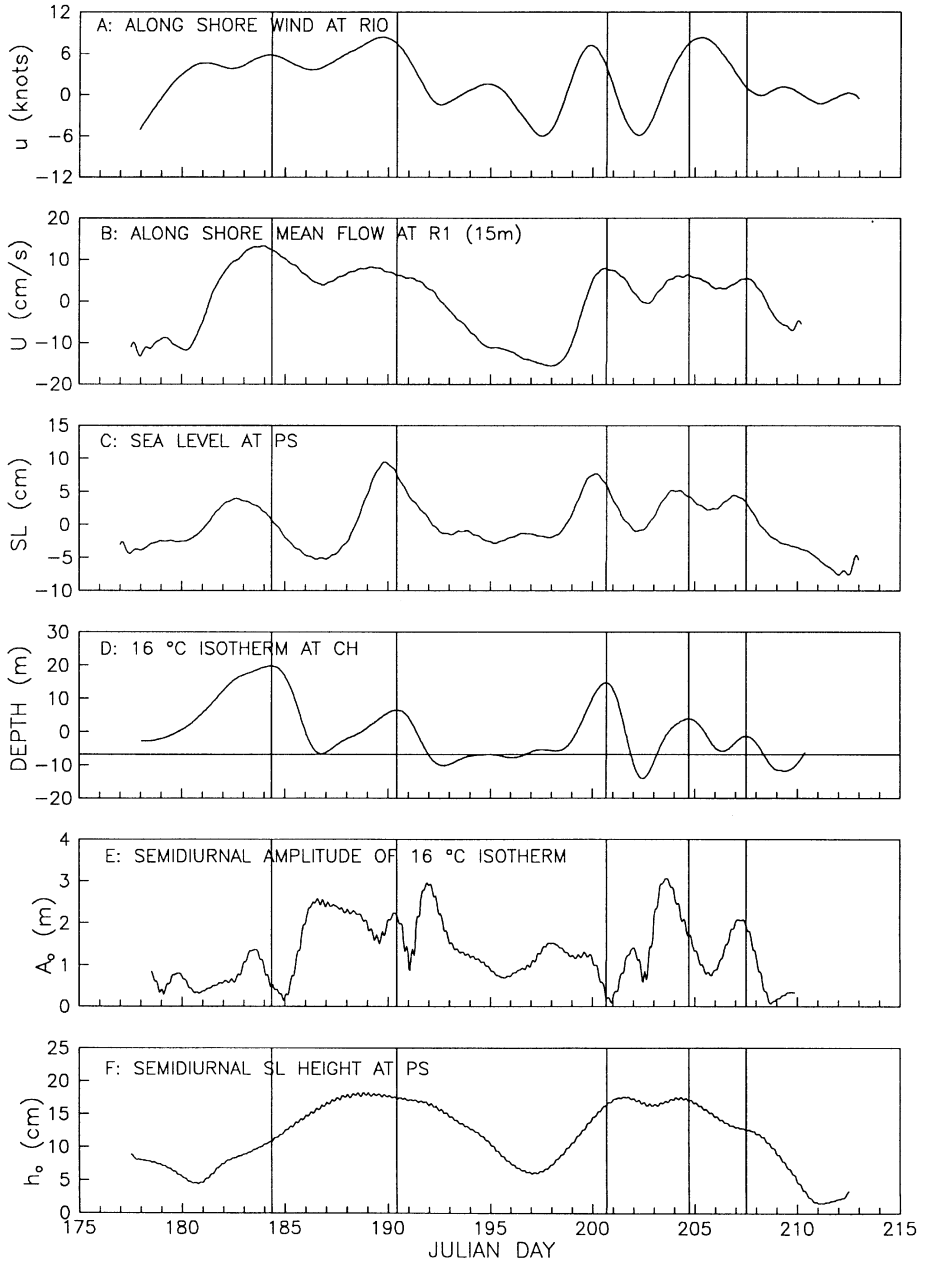

Fig. 6. SSA aperiodic components for (a) along channel wind speed at the strait of Rio (b) along channel current speed at location R1 and depth 12 m. (c) sea level at location PS. (d) depth of 16°C isotherm at location CH. Demodulated amplitude of the semidiurnal SSA component for (e) the 16°C isotherm at CH and (f) the sea level at PS.

During days 197–198 (Fig. 4) when the isotherms start to tilt, mode 3 and mode 2 start slowly to attenuate while mode 1 still builds up. Then during day 199, mode 1 follows the same pattern and finally when the tilt is at its maximum (day 200), the amplitude of the first mode reaches its minimum and a phase shift of mode 3 develops. After that, all three modes gain energy again. If this is taken to be the general case it would imply that as long as the vertical density gradient remains large, the first baroclinic mode is not affected.

6. Conclusions

The presence of internal wave of semi-diurnal period in the Gulf of Korinthos is demonstrated for the first time. The generation of the internal waves is due to the interaction of the strong tidal currents with the bottom step topography near Navpaktos Bay. Most of the energy (80%), lies in the first mode, while three modes were enough to describe adequately the vertical profile.

In theory, the internal tide is expected to behave as a Kelvin wave propagating in both directions, (eastward and westward), away from the generation region. Nevertheless, the difference of the barotropic tidal currents at stations R1 and R2 and the incoherent baroclinic modes at these two stations contradict this suggestion. Under certain conditions (Forrester 1974), lateral oscillations are also permitted. For the present case, this can be materialised only if c_n is less than $0.17\,m\,s^{-1}$ in the Gulf of Patras and Navpaktos and less than $0.34\,m\,s^{-1}$ in the Gulf of Korinthos. The numerical solution of the Sturm Liouville equation showed that this condition is realisable only for modes higher than 3 contradicting the observed modal energy distribution. Although it is impossible to resolve the problem on the basis of the present data set it is worth pointing out the possible presence of evanescent Poincaré waves which decay in the along channel direction. As shown by Brown (1973) and Middleton (1991), such waves can be found at the mouths of straits and gulfs and can profoundly effect the local circulation, even though they do not transport energy along the channel.

During strong upwelling and downwelling events, the baroclinic energy totally disappeared do to destruction of the stratification. The higher modes dissipate faster. Longer observations are needed to resolve the problem. The analytical work should be complemented with results provided by a primitive equation numerical model applied for the entire basin, and the investigation of these processes should be revisited. The semi-enclosed nature of the channel and the resulting well controlled forcing, make it useful for investigating such phenomena and testing theoretical formulae describing them.

Acknowledgements

The current meter records were made available by the National Centre for Marine Research and the tidal gauge data were provided by the Hellenic Navy Hydrographic

Service. Comments from M.N. Tsimplis and S.E. Poulos and anonymous referees are gratefully acknowledged.

References

Baines, P.G., 1974. The generation of internal tides over steep continental slopes. Philosophical Transactions of the Royal Society London 227, 27–58.

Brown, P.J., 1973. Kelvin-wave reflection in a semi-infinate canal. Journal of Marine Research 31, 1–10.

Drakopoulos, P.G., Marsden, R.F., 1993. The internal tide off the west coast of Vancouver Island. Journal of Physical Oceanography 23, 758–775.

Foreman, M.G.G., 1977. Manual for tidal heights analysis and prediction. Pacific Marine Science Report 77–10, Institute of Ocean Sciences, Patricia Bay, 97pp.

Forrester, W.D., 1974. Internal tides in St. Lawrence estuary. Journal of Marine Research 32, 55–66.

Middleton, J.F., 1991. Coastal-trapped wave scattering into and out of Straits and Bays. Journal of Physical Oceanography 21, 681–694.

Thomson, R.E., Huggett, W.S., 1980. M_2 Baroclinic Tides in Johnstsone Strait, British Columbia. Journal of Physical Oceanography 10, 1509–1539.

Vautard, R., Yiou, P., Ghil, M., 1992. Singular-spectrum analysis. a toolkit for short, noisy chaotic signals. Physica D 58, 95–126.

Wunsch, C., 1975. Internal tides in the ocean. Review of Geophysics 13, 167–182.